pISSN 1229-3008 eISSN 2287-6251
Progress in Superconductivity and Cryogenics
Vol.26, No.1, (2024), pp.1~4 https://doi.org/10.9714/psac.2024.26.1.001

A study on design process of HTS bulk magnet synchronous motors

Jaheum Koo, JuKyung Cha, Jonghoon Yoon, and Seungyong Hahn*

Department of Electrical and Computer Engineering, Seoul National University, Seoul, Korea

(Received 19 December 2023; revised or reviewed 2 February 2024; accepted 3 February 2024)

Abstract

This study explores the use of a bulk type high-temperature superconductors (HTS) as trapped field magnets in synchronous motors. A HTS bulk is examined for its ability to generate powerful magnetic fields over a permanent magnet and to eliminate the need for a direct power supply connection compared to a tape form of HTS. A 150 kW interior-mounted bulk-type superconducting synchronous motor is designed and analyzed. The A-H formulation is used to numerical analysis. The results show superior electrical performance and weight reduction when comparing the designed model with the conventional permanent magnet synchronous motor of the same topology. This study presents HTS bulk synchronous motor's overall design process and highlights its potential in achieving relatively high power density than conventional permanent magnet synchronous motor.

Keywords: HTS synchronous machine, trapped field, bulk superconductors, pulsed field magnetization

1. INTRODUCTION

There has been a growing body of research on high-power density motors using high-temperature superconductors (HTS) [1-9]. HTS materials can be utilized as a trapped field magnet (TFM), generating a conically shaped field distribution with a high magnetic field in a bulk type. It does not require a direct connection to the power supply in the rotor part, making it a tremendous advantage in rotating machines like permanent magnet synchronous motors (PMSM) [10-12].

For the HTS bulk to be used as quasi-permanent magnet, additional magnetization process needs to be performed in the cryogenic temperature. In the partially superconducting rotating machines that use conventional copper armature windings, the magnetization process can be accomplished by discharging a capacitor bank connected to an armature winding which is called post-assembly magnetization [13]. When the capacitor bank discharges, a pulsed magnetic field is applied to the HTS bulk magnet of the rotor part. This magnetic field is trapped in their bodies. This process can be explained by flux pinning phenomenon and can be simulated using a special governing equation suitable for superconductivity and an index model representing nonlinear resistivity [14].

In this paper, 150 kW interior mounted HTS bulk superconducting synchronous motor was designed using finite element method (FEM) simulation. 'Interior-mounted' refers to the configuration in which magnets are installed inside the rotor yoke. Based on the 2D magnetic analysis, The governing equations of the A-H formulation used in the analysis were explained. Furthermore, some of details about the design process of this type of HTS bulk synchronous motor were provided, considering the magnetization process and synchronous operating state.

* Corresponding author: hahnsy@snu.ac.kr

Finally, the electrical performances of our designed HTS bulk synchronous motor with a conventional PMSM of the same topology and mechanical output power focusing on motor active part weight were compared.

2. TOPOLOGY DESIGN

Type-II superconductors have flux pinning property which can hold the penetrated magnetic flux in their bodies even after an external field is removed. REBCO HTS bulk has strong pinning properties that can trap over 2 T in their bodies and act as quasi-permanent magnet [15]. In the perspective of rotating machine design, a magnet capable of trapping over 2 T is highly advantageous as it is unattainable by permanent magnets (PM). It can increase the power density and reduce additional loss due to the brush. This performance evaluation was conducted using COMSOL Multiphysics.

2.1. Topology of Designed Model

Fig. 1 displays the designed HTS bulk-type synchronous motor. The initial topology is an 8-pole, 24-slot, interior-mounted synchronous motor with an overall stator diameter of 250 mm. The armature employs a 3-phase hairpin-type concentrated winding with high slot fill factor 0.7 [16], considering magnetization process. Both the stator and rotor yokes are constructed with laminated iron core 35PN230. The rotor magnet is assumed as a HTS bulk 22.7 mm × 6.8 mm in size magnets, and this size is determined through an initial magnetization FEM analysis considered a magnitude of pulsed field and HTS bulk performance. Also, a parametric sweep was done using the stator yoke design parameters to reduce torque ripple and potential noise problems [17, 18] considering a conical shape magnetic flux density distribution of HTS bulk.

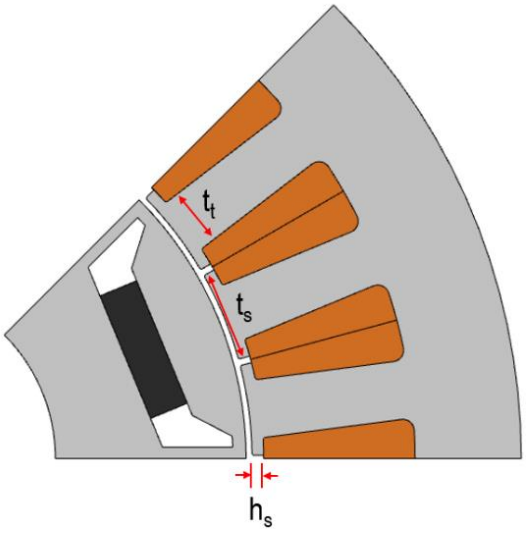

Fig. 1. Designed interior mounted magnet motor 1/8th model and design parameters for parametric sweep.

Final design was selected using the parametric sweep with FEM based on the thickness and height of tooth and shoe in the stator core which can affect torque ripple. All design results are assumed: 1) 10 A_{peak}/mm^2 armature current density; and 2) synchronous state in the same initial mechanical angle and rotating speed. The values were selected t_t = 10 mm; t_s = 16 mm; h_s = 2 mm.

3. MODELLING AND ELECTRICAL PERFORMANCE CALCULATION

3.1. Governing Equation in the FEM Analysis

In quasi-static magneto analysis, the A-formulation is typically used, which is based on a magnetic vector potential $\boldsymbol{A}$. The governing equation of the A-formulation is expressed in (1), derived from the Maxwell equation.

$$\sigma \frac{\partial \boldsymbol{A}}{\partial t} - \frac{1}{\mu}\nabla^2 \boldsymbol{A} = \boldsymbol{J} \qquad (1)$$

Here, σ represents electrical conductivity, and μ represents permeability. $\boldsymbol{A}$ and $\boldsymbol{J}$ denote the magnetic vector potential and electrical current density, respectively.

The A-formulation is powerful equation widely used in FEM analysis of electrical rotating machines. However, it is not suitable for calculating nonlinear resistivity and extremely high electrical conductivity such as superconductors. To represent the flux pinning property in HTS bulk, The H-formulation [19-21] was adopted for the superconducting region based on a magnetic field intensity $\boldsymbol{H}$, as shown in (2).

$$\mu \frac{\partial \boldsymbol{H}}{\partial t} + \nabla \times \boldsymbol{E} = 0 \qquad (2)$$

$\boldsymbol{E}$ represents the electrical field vector in this equation. The H-formulation is well-established in various papers for its usefulness in FEM analysis of superconductivity. In the H-formulation, the nonlinear resistivity is represented by following equation.

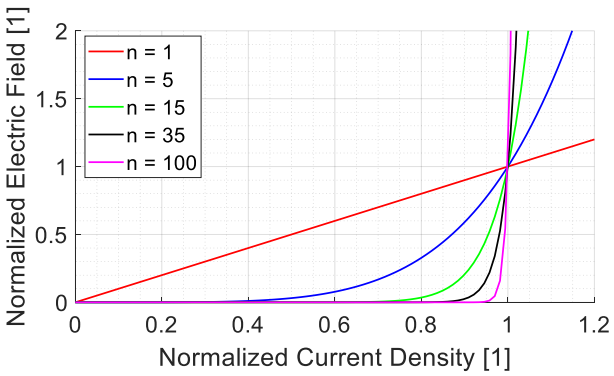

Fig. 2. Normalized current density vs electric field graph in index model.

$$E = E_c \left(\frac{J}{J_c}\right)^n \qquad (3)$$

In the (3), E_c represents the characteristic electric field, conventionally assumed to be 1 μV/cm, J_c represents critical current density of superconductor, and n represents the index number, which varies depending on superconductivity. In the index model, the 'n' parameter plays a critical role, influencing the superconducting transition in FEM. A higher 'n' value implies a more abrupt or sudden shift from the normal to the superconducting state.

Fig. 2 displays a graph illustrating the relationship between the electrical field and the magnitude of the current density within a superconductor. The x- and y-axis of the graph are normalized to represent the characteristic electric field and critical current density, respectively. This relationship between the electric field and current density was used to implement nonlinear resistive behavior in this model [22]. This index model also has been generally agreed well around near the resistive transition of superconductor. Within the scope of this study, the n value, denoting a specific parameter within this model, was set to 35.

Moreover, to integrate the A and H-formulation, at their boundaries, coupling conditions were applied using a weak contribution setting [23]. This approach was chosen to ensure convergence within the COMSOL Multiphysics.

$$\begin{aligned} &\text{A-formulation: } \boldsymbol{H}_t \cdot test(\boldsymbol{A}_z) \\ &\text{H-formulation: } \boldsymbol{E}_z \cdot test(\boldsymbol{H}_t) \end{aligned} \qquad (4)$$

$\boldsymbol{H}_t$ and $\boldsymbol{A}_z$ mean tangential $\boldsymbol{H}$ vector in the boundary and $\boldsymbol{A}$ vector in z-axis respectively. $test$ is test function operator in the FEM program COMSOL Multiphysics to model the weak form between two formulations. Equation (4) means the tangential $\boldsymbol{H}$ vector acts as a source of A-formulation and the $\boldsymbol{E}$ vector acts as a source of H-formulation in this coupled simulation.

Fig. 3 means the regions and boundaries of each formulation in this simulation, The H-formulation was only used in the superconducting region of the rotor magnet part and coupled around the edge of HTS bulk magnet with external A-formulation regions using the equation (3) to analyze the electrical performance of

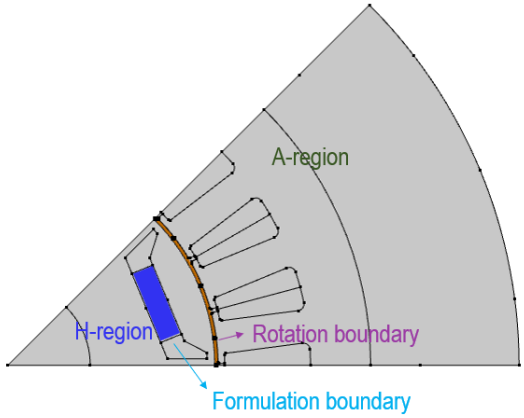

Fig. 3. Model setting for A-H formulation study.

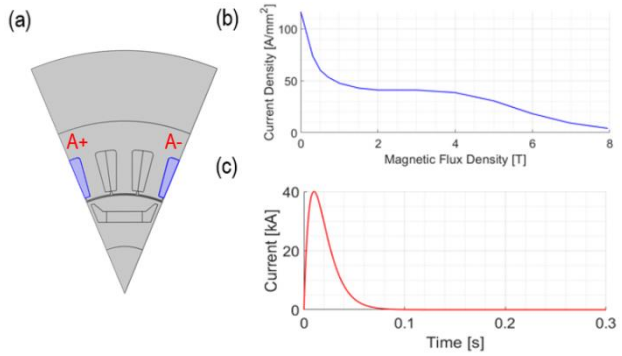

Fig. 4. Analysis settings in magnetization process: (a) A phase winding; (b) critical current density of HTS bulk; (c) input pulsed current in A phase winding.

superconducting rotating machines.

3.2. Magnetization Process

HTS REBCO bulk have a critical current density that depends on temperature and magnetic field. To apply trapped field characteristics in HTS bulk-type motor, an additional magnetization process must be applied during every operation at cryogen temperatures. Since it is nearly impossible to magnetize the HTS bulk before the install in the motor with a high magnetic field at cryogenic temperatures, magnetization of HTS bulk-type motor can only be achieved by applying a current to the armature winding.

Fig. 4(a) shows the A phase windings. The section highlighted in blue represents the winding for A phase. Fig. 4(b) is the bulk REBCO transport critical current measurement data in 77 K at Robinson Research Institute [24]. Fig. 4(c) is armature windings input current graph in the magnetization process. Post-assembly magnetization typically involves an instantaneous discharge from a bank capacitor device known as pulsed field magnetization (PFM) [25]. Magnetizing current was applied only to A phase of armature windings in Fig. 4(a), assuming a time constant of 10 ms and a peak current of 40 kA.

Fig. 5 represents post assembly magnetization simulation results. Fig. 5(a) shows overall magnetic flux distribution. Fig. 5(b) mean the induced and current density distribution in the HTS bulk after magnetization process.

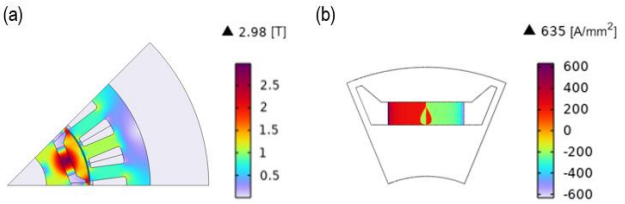

Fig. 5. Analysis results after magnetization process: (a) magnetic flux density distribution of motor; and (b) current density distribution in the HTS bulk after magnetization.

The HTS bulk within the iron core was magnetized to 2.98 T peak value and 1.76 T average value in 77 K, and this value is nearly impossible with a conventional permanent magnet. The bulk HTS can enhance the power density of superconducting rotating machines more than PMSM with this high magnetic performance.

3.3. Electrical Performance Comparison Between HTS bulk-type motor and PM-type motor

After calculating the current density distribution in the HTS bulk resulting from the magnetization process using 2D FEM, the torque performance was computed in a synchronous rotating state. PM-type motor of the same topology was calculated manually to compare HTS bulk-type synchronous motors performance value. In the PM-type model, the permanent magnet in the rotor was defined as having a uniform residual magnetic flux magnitude of 1.40 T in radial direction. These results are summarized in Table. 1.

With the torque value obtained from the synchronous rotating model, the required stack length with a performance of 150 kW in 6000 r/min of two models was determined respectively. In the HTS bulk-type synchronous motor model, this stack lengths were calculated to be 177.8 mm, and in the PM-type model, it was 214.9 mm. Also, the weights of two models were calculated based on density and stack length of active parts.

The overall wights are 43.6 kg and 53.2 kg, respectively. In a cryogenic environment, when submerged in liquid nitrogen, simply replacing the PM with HTS bulk means that the active parts of motor can be 21.0% lighter and 16.5 % smaller in volume. Finally, several types of loss and efficiencies of each model were calculated: (A) iron loss

TABLE I
MOTORS PERFORMANCE TABLE.

Parameters	Units	HTS bulk-type	PM-type
Power	[kW]	150	
Torque	[Nm]	238.7	
Rotating speed	[r/min]	6000	
Poles; Slots; Phases	[-]	8; 24; 3	
Overall diameter	[mm]	220	
Stack length	[mm]	177.8	214.9
Weight*	[kg]	43.6	53.2
Operating temperature	[K]	77	
Overall loss	[W]	2999.6	3200.5
Efficiency	[%]	98.0	97.9
Armature Winding			
Winding type	[-]	Hair-pin copper winding	
Number of turns per slots	[-]	7	
Slot fill factor	[-]	0.7	
Rotor magnet			
Material	[-]	Bulk REBCO	NbFeB
Maximum flux density value	[T]	2.98	1.40

* Only active parts are considered

which occur in the iron yoke employing the Steinmetz equation to calculate hysteresis loss and (B) copper loss which occur in the armature copper wire considering the reduction of electrical resistivity in a cryogenic temperature. Due to the difference in stack length, the HTS bulk-type motor shows reduced iron and copper losses compared to the PM-type motor. As a result, considering the given output and loss values, the calculated efficiency for each model, were 98.0% and 97.9% respectively.

4. CONCLUSION

This research presents the significant potential of integrating HTS bulk as a rotor magnet. During the parametric sweep process, design parameters based on the length and height of stator yoke components were defined and selected. Additionally, because of the characteristics of HTS bulk, the additional magnetization model was composed to design the HTS bulk synchronous motor. For calculation of electrical performances in synchronous rotating situation, we conducted a comparative analysis between the HTS bulk-type motor and PM-type motor. Our study proposed an overall design method for HTS bulk in rotating machines considering the trapped field characteristics and explored the possibility of replacement for permanent magnets that can achieve lower weight at the same mechanical performance.

Furthermore, we can also anticipate that a more advantageous design for HTS bulk-type motors by considering the HTS armature and air-core type stator yoke which means fully superconducting brushless rotating machines, eliminating the capacitor bank, iron losses and even brushes around a rotating part.

ACKNOWLEDGMENT

This work was supported in part by National R&D Pro gram through the National Research Foundation of Korea (NRF) funded by Ministry of Science and ICT(2022M3I9 A1073924), in part by National R&D Program through th e National Research Foundation of Korea(NRF) funded b y Ministry of Science and ICT(2022M3I9A1072846), and in part by the Applied Superconductivity Center, Electric Power Research Institute of Seoul National University.

REFERENCES

[1] J. J. Scheidler and T. F. Tallerico, “Design, fabrication, and critical current testing of no-insulation superconducting rotor coils for NASA’s 1.4 MW high-efficiency megawatt motor,” *2018 AIAA/IEEE Electric Aircraft Technologies Symposium (EATS)*, pp. 1-9, Jul. 2018.

[2] G. Snitchler, B. Gamble, and S. Kalsi, “The performance of a 5 MW high temperature superconductor ship propulsion motor,” *IEEE Trans. Appl. Supercond.*, vol. 15, no. 2, pp. 2206-2209, 2005.

[3] D. S. Dezhin and I. N. Dezhina, “Development of the future aircraft propulsion system based on HTS electrical equipment with liquid hydrogen cooling,” *IEEE Trans. Appl. Supercond.*, vol. 32, no. 4, pp. 1-5, 2022.

[4] R. Dorget, et al., “Design of a 500 kW partially superconducting flux modulation machine for aircraft propulsion,” *J. Phys.: Conf. Ser.*, vol. 1975, no. 1, pp. 012033, Jul. 2021.

[5] H. Sasa, et al., “Experimental evaluation of 1 kW-class prototype REBCO fully superconducting synchronous motor cooled by subcooled liquid nitrogen for e-aircraft,” *IEEE Trans. Appl. Supercond*, vol. 31, no. 5, pp. 1-6, 2021.

[6] M. Zhang, F. Eastham, and W. Yuan, “Design and modeling of 2G HTS armature winding for electric aircraft propulsion applications,” *IEEE Trans. Appl. Supercond*, vol. 26, no. 3, pp. 1-5, 2016.

[7] U. Bong, et al., “Investigation on key parameters of NI HTS field coils for high power density synchronous motors,” *IEEE Trans. Appl. Supercond*, vol. 31, no. 5, pp. 1-5, 2021.

[8] S. Fukui, et al., “Numerical study of optimization design of high temperature superconducting field winding in 20 MW synchronous motor for ship propulsion,” *IEEE Trans. Appl. Supercond*, vol. 22, no. 3, pp. 5200504-5200504, 2012.

[9] Y. Gao and T. Nakamura, “Design and performance analysis of 25 kw class HTS induction/synchronous motor with self-organizing method for transportation applications,” *IEEE Trans. Appl. Supercond*, vol. 33, no. 5, pp. 1-7, 2023.

[10] Y. Zhang, D. Zhou, T. Ida, M. Miki, and M. Izumi, “Meltgrowth bulk superconductors and application to an axial-gaptype rotating machine,” *Supercond. Sci. Technol*, vol. 29, no. 4, pp. 044005, 2016.

[11] M. Watasaki, et al., “Stability model of bulk HTS field pole of a synchronous rotating machine under load conditions,” *Supercond. Sci. Technol*, vol. 34, no. 3, pp. 035015, 2021.

[12] Z. Huang, M. Zhang, W. Wang, and T. A. Coombs, “Trial test of a bulk-type fully HTS synchronous motor,” *IEEE Trans. Appl. Supercond*, vol. 24, no. 3, pp. 1-5, 2014.

[13] D. G. Dorrell, M. -F. Hsieh, and Y. -C. Hsu, “Post assembly magnetization patterns in rare-earth permanent-magnet motors,” *IEEE Trans. Magn.*, vol. 43, no. 6, pp. 2489-2491, 2007.

[14] Y. Iwasa, *Case Studies in Superconducting Magnets: Design and Operational Issues*. Springer US, 2009.

[15] J. H. Durrel, et al., “A trapped field of 17.6 T in melt-processed, bulk Gd-Ba-Cu-O reinforced with shrink-fit steel,” *Supercond. Sci. Technol*, vol. 27, no. 8, pp. 082001, 2014.

[16] A. Arzillo. et al., “An analytical approach for the design of innovative hairpin winding layouts,” *2020 International Conference on Electrical Machines (ICEM)*, vol. 1, pp. 1534-1539, Aug. 2020.

[17] D. Wang, C. Peng, J. Li, and C. Wang, “Comparison and experimental verification of different approaches to suppress torque ripple and vibrations of interior permanent magnet synchronous motor for EV,” *IEEE Trans. Ind. Electron*, vol. 70, no. 3, pp. 2209-2220, 2023.

[18] C. Peng, D. Wang, Z. Feng, and B. Wang, “A new segmented rotor to mitigate torque ripple and electromagnetic vibration of interior permanent magnet machine,” *IEEE Trans. Ind. Electron*, vol. 69, no. 2, pp. 1367-1377, 2022.

[19] M. Ainslie and H. Fujishiro, *Numerical Modelling of Bulk Superconductor Magnetisation*, ser. 2053-2563. IOP Publishing, 2019.

[20] F. Sass, G. G. Sotelo, R. de Andrade Junior, and F. Sirois, “H-formulation for simulating levitation forces acting on HTS bulks and stacks of 2g coated conductors,” *Supercond. Sci. Technol*, vol. 28, no. 12, pp. 125012, 2015.

[21] B. Shen, F. Grilli, and T. A. Coombs., “Review of the AC loss computation for HTS using H formulation,” *Supercond. Sci. Technol*, vol. 33, no. 3, pp. 033002, 2021.

[22] Y. Iwasa and V. Y. Adzovie, “Index number (n) below “critical” current in Nb-Ti superconductors,” *IEEE Trans. Appl. Supercond*, vol. 5, no. 3, pp. 3437-3441, 1995.

[23] R. Brambilla, F. Grilli, L. Martini, M. Bocchi, and G. Angeli, “A finite element method framework for modeling rotating machines with superconducting windings,” *IEEE Trans. Appl. Supercond*, vol. 28, no. 5, pp. 1-11, 2018.

[24] R. W. Taylor, et al., “Transport current measurement of Ic(T, B,θ) and n(T, B,θ) for a bulk REBCO superconductor,” *IEEE Trans. Appl. Supercond*, vol. 33, no. 5, pp. 1-6, 2023.

[25] Z. Huang, H. S. Ruiz, Y. Zhai, J. Geng, B. Shen, and T. A. Coombs, “Study of the pulsed field magnetization strategy for the superconducting rotor,” *IEEE Trans. Appl. Supercond*, vol. 26, no. 4, pp. 1-5, 2016.